

1 **Supplement of “Formation of Highly Absorptive Secondary Brown Carbon**  
2 **Through Nighttime Multiphase Chemistry of Biomass Burning Emissions”**

3 **Ye Kuang<sup>1,\*</sup>, Biao Luo<sup>1</sup>, Shan Huang<sup>1\*</sup>, Junwen Liu<sup>1</sup>, Weiwei Hu<sup>2</sup>, Yuwen Peng<sup>1</sup>, Duohong Chen<sup>3</sup>,**  
4 **Dingli Yue<sup>3</sup>, Wanyun Xu<sup>4</sup>, Bin Yuan<sup>1</sup>, Min Shao<sup>1</sup>**

5 <sup>1</sup> Institute for Environmental and Climate Research, College of Environment and Climate, Jinan  
6 University, Guangzhou, China..

7 <sup>2</sup> State Key Laboratory of Organic Geochemistry and Guangdong Key Laboratory of Environmental  
8 Protection and Resources Utilization, Guangzhou Institute of Geochemistry, Chinese Academy of  
9 Sciences, Guangzhou 510640, China

10 <sup>3</sup> Guangdong Ecological and Environmental Monitoring Center, State Environmental Protection Key  
11 Laboratory of Regional Air Quality Monitoring, Guangzhou 510308, China

12 <sup>4</sup> State Key Laboratory of Severe Weather, Key Laboratory for Atmospheric Chemistry, Institute of  
13 Atmospheric Composition, Chinese Academy of Meteorological Sciences, Beijing, China

14

15 Corresponding author: Ye Kuang ([kuangye@jnu.edu.cn](mailto:kuangye@jnu.edu.cn)) and Shan Huang

16 ([shanhuang\\_eci@jnu.edu.cn](mailto:shanhuang_eci@jnu.edu.cn))

17

18

19

20

21

22

23

24

25 **1. Methods**

26 **1.1 Aerosol liquid water content calculations**

27 The size resolved aerosol liquid water content (ALWC) was formulated as the following in which  
28 the ALWC was the summation of aerosol water contributed by inorganic aerosols and organic aerosols:

29 
$$ALWC(D_a) = ALWC_{Inorg}(D_a) + ALWC_{org}(D_a)$$

30 Where the  $ALWC_{Inorg}(D_a)$  was calculated using the ISORROPIA (Kuang et al., 2018) model using  
31 reverse mode and metastable with size resolved inorganic aerosol chemical compositions measured by  
32 the SP-AMS as inputs. The  $ALWC_{org}(D_a)$  was calculated as:

33 
$$ALWC_{org}(D_a) = \frac{m_{org}(D_a)}{\rho_{org}} \times \rho_w \times \frac{\kappa_{org}}{\left(\frac{100\%}{RH} - 1\right)}$$

34 The  $m_{org}(D_a)$  is the size resolved organic aerosol mass concentrations measured by the SP-AMS,  
35 the  $\kappa_{org}$  derived in Kuang et al. (2021) was used.

36

37

38

39

40

41

42

43

44

45

46

47

48

49

50

51

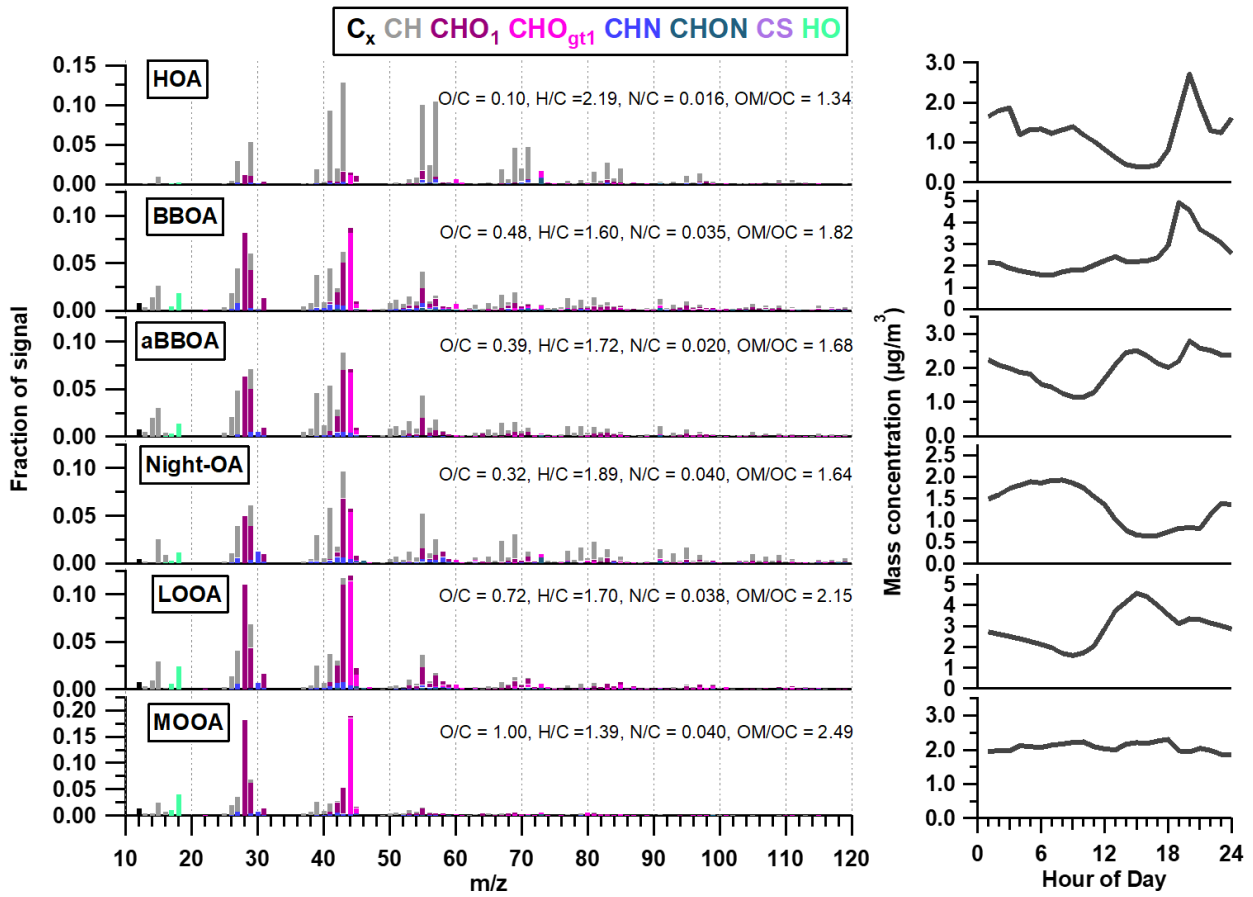
52

53

54

55 **2. Supplementary Figures**

56  
57  
58  
59



60

61 **Figure S1.** Mass spectral profile and diurnal variation of PMF factors based on SP-AMS measurements, note that the O/C  
62 of HOA here is different with that in Luo et al. (2022) because of the mislabeling and corrected here.

63  
64  
65  
66  
67  
68  
69  
70  
71  
72  
73  
74  
75  
76

77  
78  
79  
80  
81  
82  
83  
84  
85

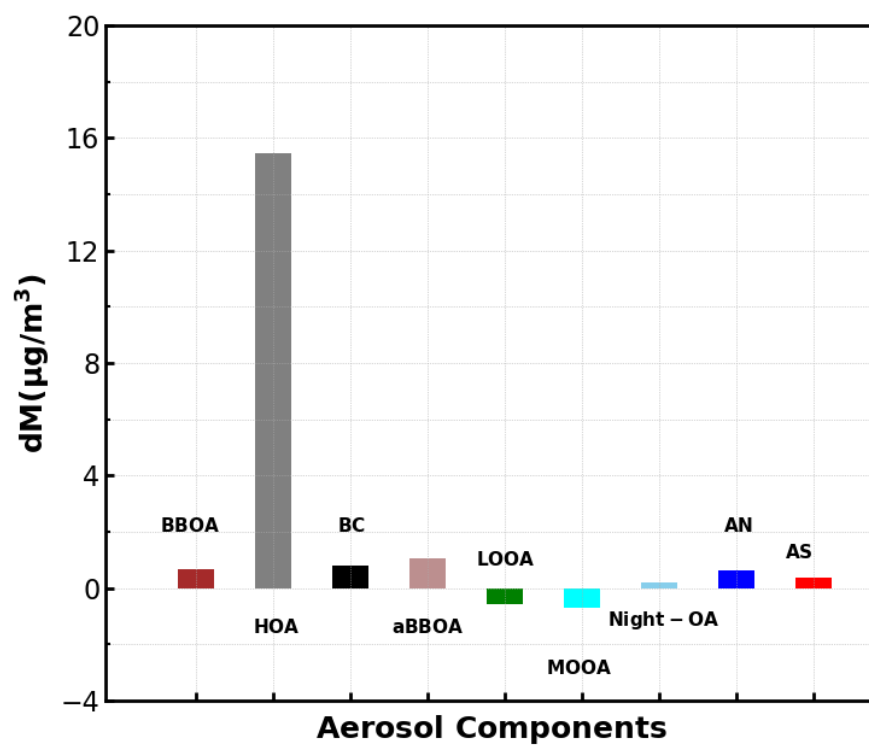


**Figure S2.** Average mass concentration changes of aerosol components for identified HOA increase cases, AN represents ammonium nitrate and AS represents ammonium sulfate.

86  
87  
88  
89  
90  
91

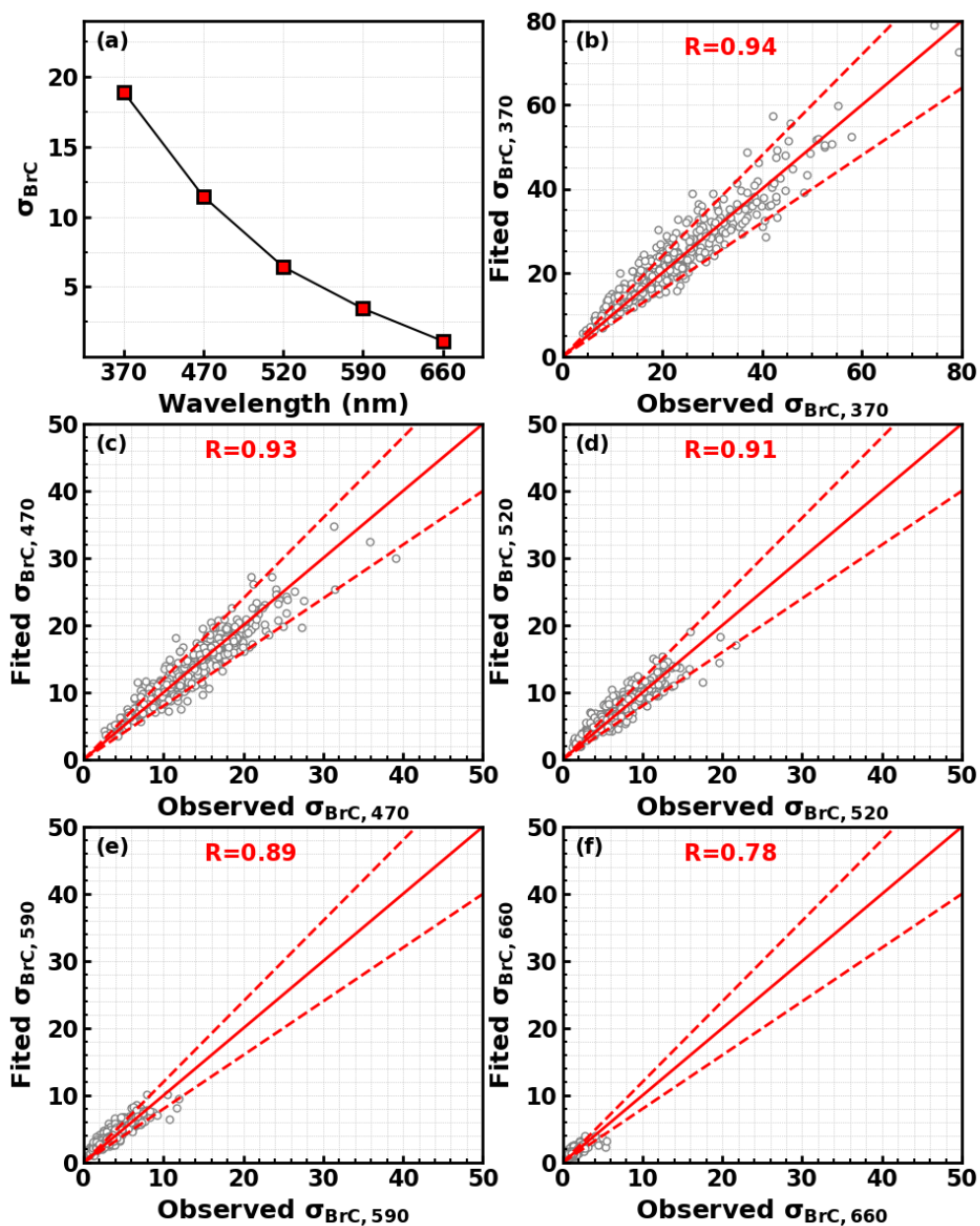


Figure S3. (a) Average BrC absorptions at different wavelengths, (b-f) Comparisons between predicted and observed BrC absorption values at wavelengths of 370 nm, 470 nm, 520 nm, 590 nm, and 660 nm using the multivariate linear regression method.

92  
93  
94  
95  
96  
97  
98  
99  
100

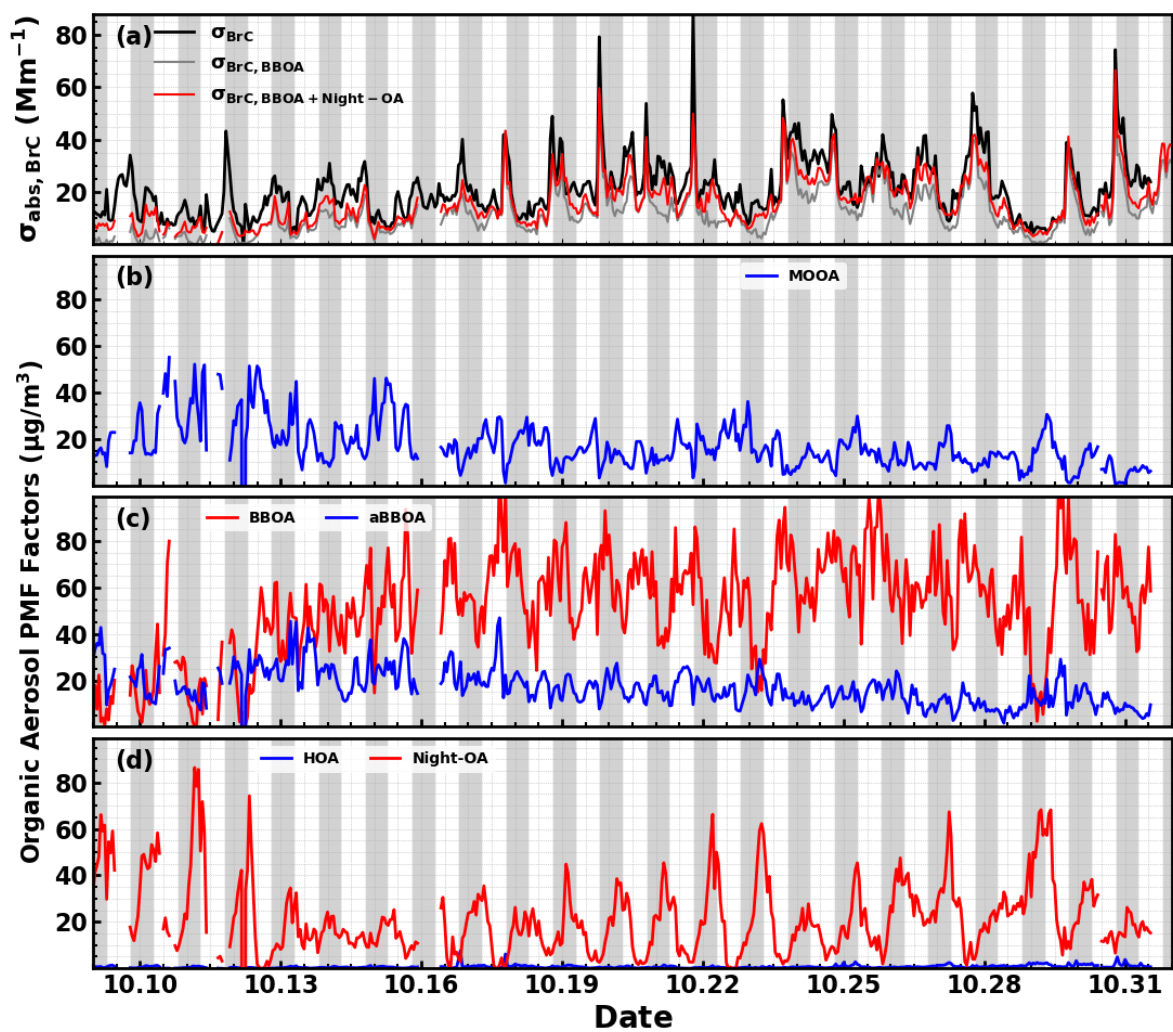


Figure S4. Timeseries of contributions of different OA factors to BrC absorption at 370 nm.

102  
 103  
 104  
 105  
 106  
 107  
 108  
 109  
 110  
 111  
 112  
 113  
 114  
 115  
 116  
 117

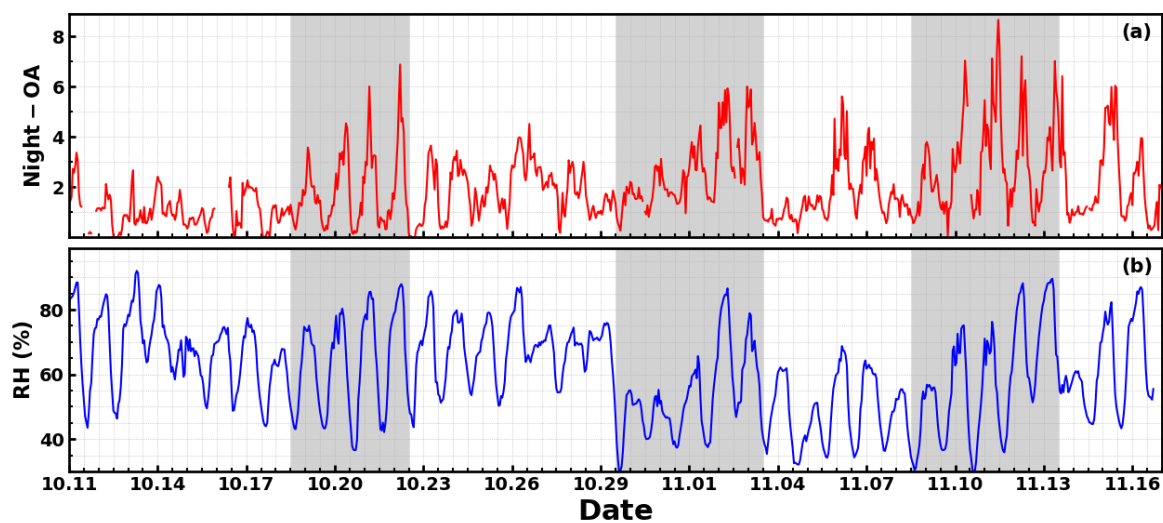


Figure S5. Timeseries of (a) Night-OA mass concentrations and (b) relative humidity (RH). Gray shading areas represent periods with remarkable Night-OA formations.

119

120

121

122

123

124

125

126

127

128

129

130

131

132

133

134

135

136

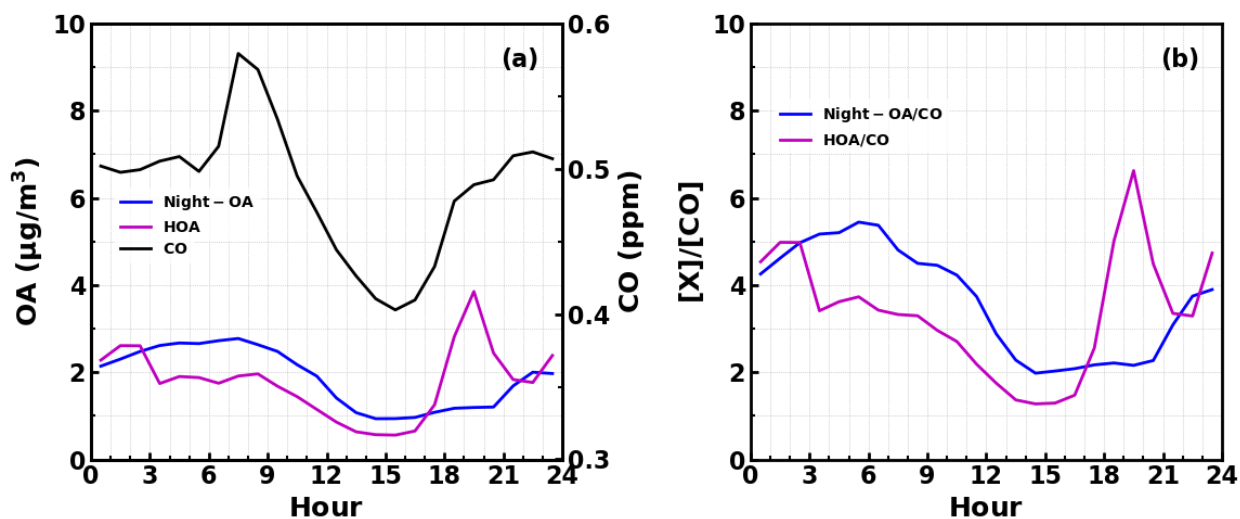


Figure S6. (a) Average diurnal variations of Night-OA, HOA and CO; (b) Average diurnal variations of  $[\text{Night-OA}]/[\text{CO}]$  and  $[\text{HOA}]/[\text{CO}]$

138

139

140

141

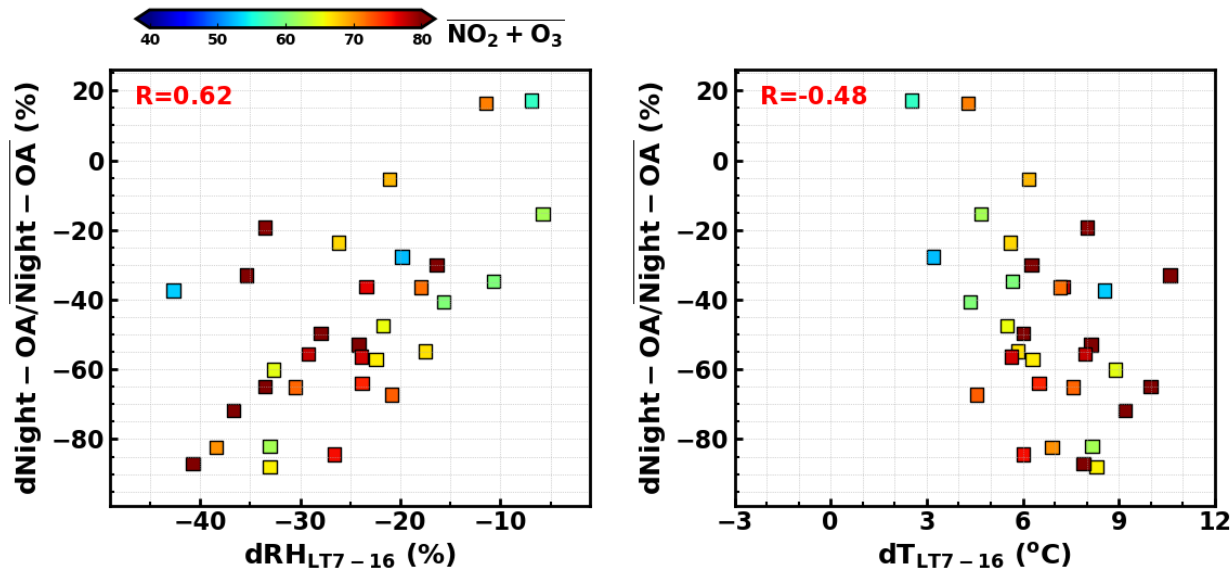


Figure S7. (a) Correlations between Night-OA decrease and RH changes from local time 07:00 in the morning to 16:00 in the afternoon; (b) Correlations between Night-OA decrease and air temperature (T) changes from local time 07:00 in the morning to 16:00 in the afternoon. Colors of square markers represent Ox ( $\text{NO}_2 + \text{O}_3$ ) levels.

142

143

144

145



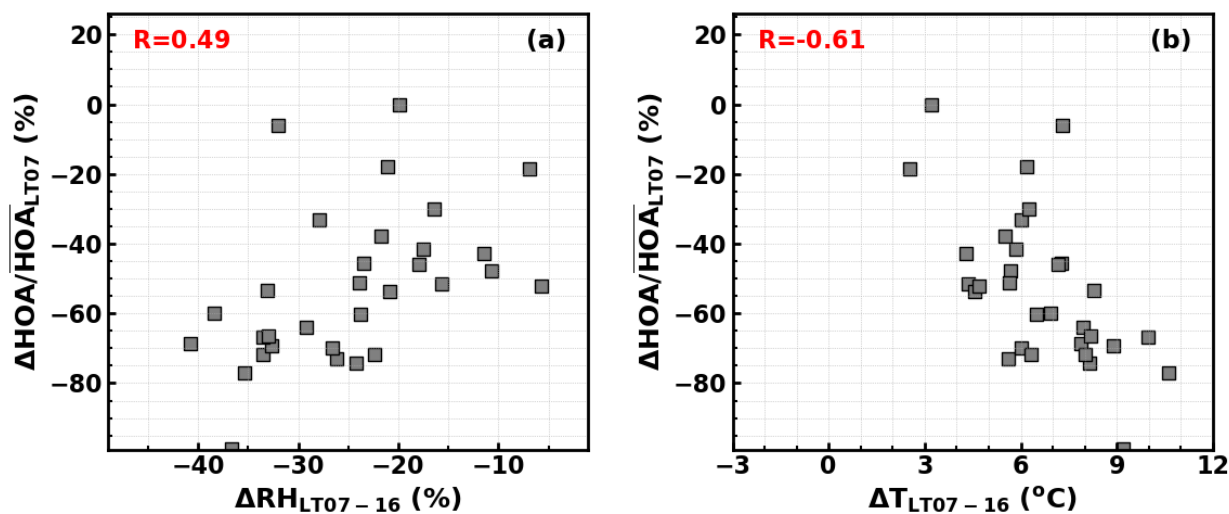


Figure S8. (a) Correlations between HOA decrease and RH changes from local time 07:00 in the morning to 16:00 in the afternoon; (b) Correlations between HOA decrease and air temperature (T) changes from local time 07:00 in the morning to 16:00 in the afternoon.

146  
147  
148  
149  
150

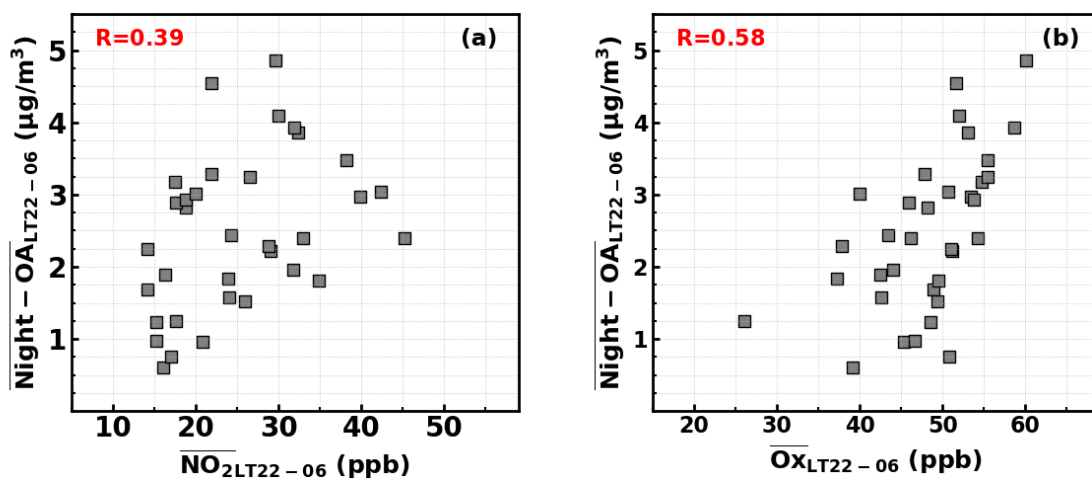
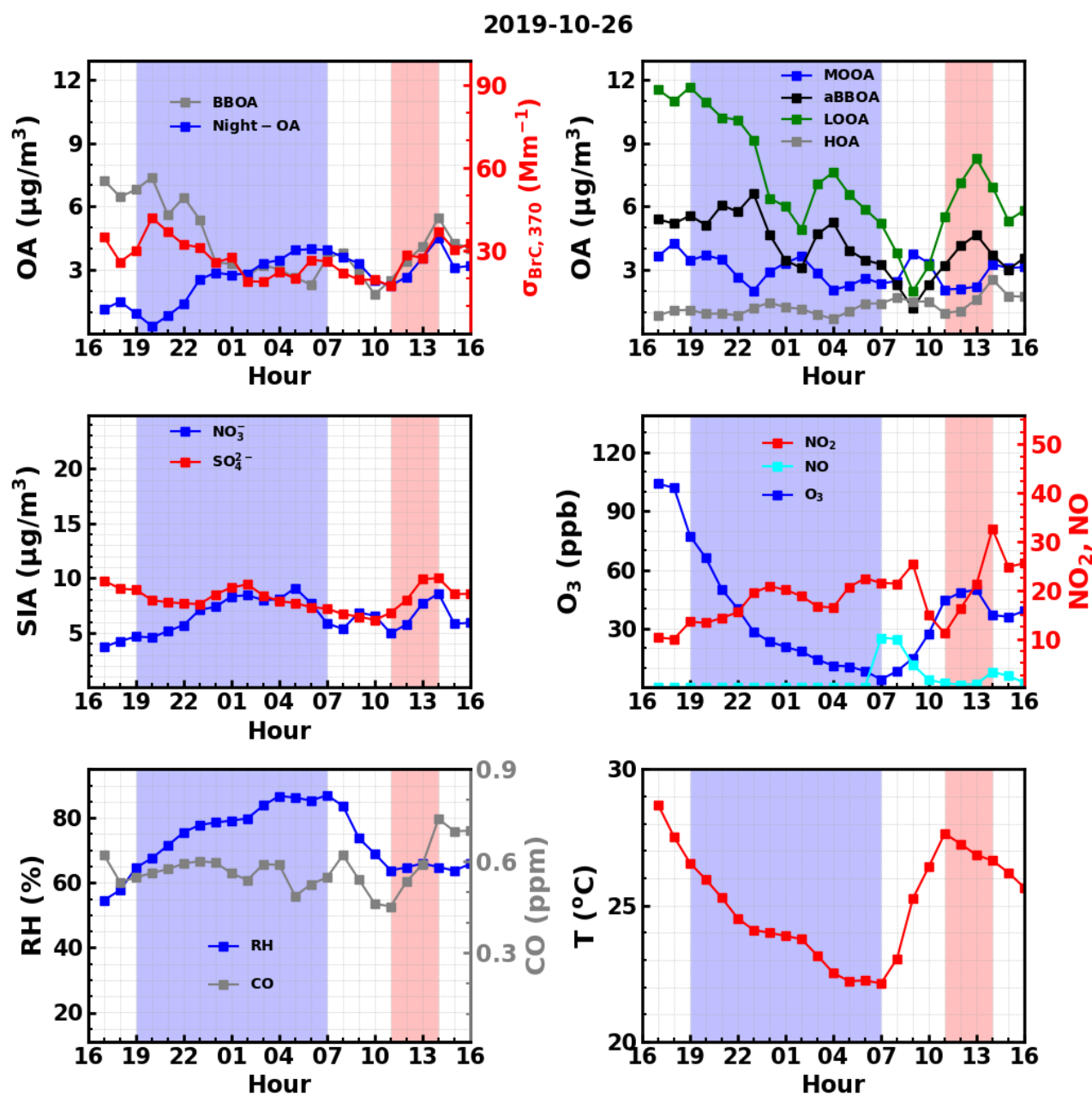


Figure S9. (a) Correlations between average Night-OA mass concentration (local time 22:00 to 06:00 of next morning) and corresponding average NO<sub>2</sub> concentration; (b) Correlations between average Night-OA mass concentration (local time 22:00 to 06:00 of next morning) and corresponding average Ox (NO<sub>2</sub>+O<sub>3</sub>) concentration.

151  
152  
153



**Figure S10.** Evolution of aerosol chemical compositions,  $\text{NO}_2$ ,  $\text{O}_3$ ,  $\text{NO}$ ,  $\text{CO}$ , and meteorological parameters such as RH and T from local time 16:00 of 25<sup>th</sup> 10, 2019 to 16:00 of 26<sup>th</sup> 10, 2019, blue shading areas represent nighttime and pink shading areas corresponding to periods with obvious daytime Night-OA increase.

155

156

157

158

159

160

2019-11-11

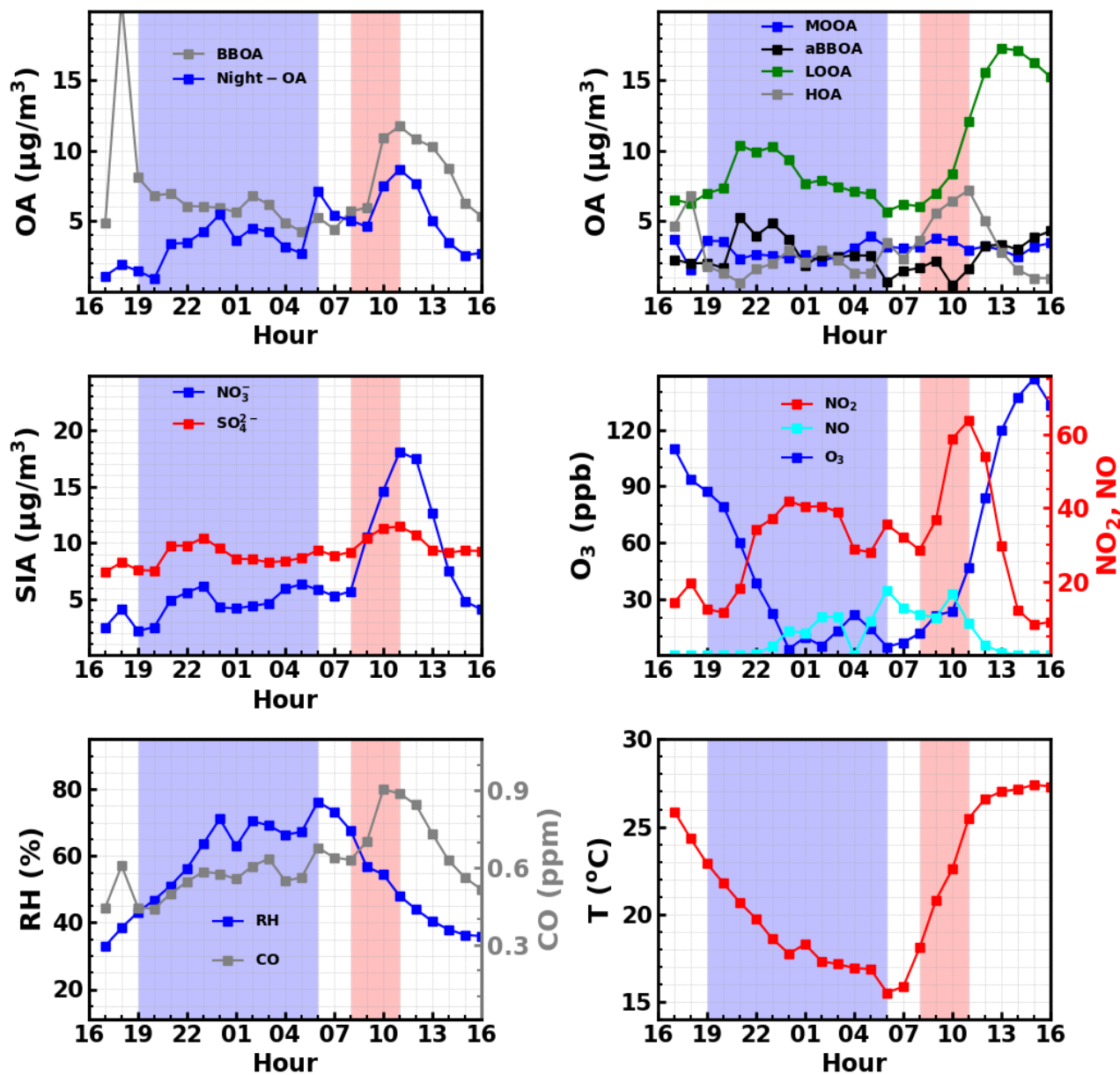


Figure S11. Evolution of aerosol chemical compositions,  $\text{NO}_2$ ,  $\text{O}_3$ ,  $\text{NO}$ ,  $\text{CO}$ , and meteorological parameters such as RH and T from local time 16:00 of 10<sup>th</sup> 11, 2019 to 16:00 of 11<sup>th</sup> 11, 2019, blue shading areas represent nighttime and pink shading areas corresponding to periods with obvious daytime Night-OA increase.

162

163

164

165

166

167

168

169 **References:**  
170 Kuang, Y., Zhao, C. S., Zhao, G., Tao, J. C., Xu, W., Ma, N., and Bian, Y. X.: A novel method for calculating ambient aerosol  
171 liquid water content based on measurements of a humidified nephelometer system, *Atmospheric Measurement*  
172 *Techniques*, 11, 2967-2982, 10.5194/amt-11-2967-2018, 2018.  
173 Kuang, Y., Huang, S., Xue, B., Luo, B., Song, Q., Chen, W., Hu, W., Li, W., Zhao, P., Cai, M., Peng, Y., Qi, J., Li, T., Chen, D., Yue,  
174 D., Yuan, B., and Shao, M.: Contrasting effects of secondary organic aerosol formations on organic aerosol hygroscopicity,  
175 *Atmos. Chem. Phys. Discuss.*, 2021, 1-27, 10.5194/acp-2021-3, 2021.  
176 Luo, B., Kuang, Y., Huang, S., Song, Q., Hu, W., Li, W., Peng, Y., Chen, D., Yue, D., Yuan, B., and Shao, M.: Parameterizations  
177 of size distribution and refractive index of biomass burning organic aerosol with black carbon content, *Atmos. Chem. Phys.*,  
178 22, 12401-12415, 10.5194/acp-22-12401-2022, 2022.  
179